Title: Design & Manufacture of a High Performance Bicycle Crank by Additive Manufacturing

Author List and Affiliations:

Iain McEwen, Innovate 2 Make Ltd, Kings Norton Business Centre, Birmingham, B30 3HP, UK. iain@mcewenfamily.co.uk

David E Cooper; Progressive Technology Ltd, Hambridge Lane, Newbury RG14 5TS, UK. dave.cooper@progressive-technology.co.uk

Jay Warnett; WMG, University of Warwick, Coventry, CV4 7AL, UK. J.M.Warnett@warwick.ac.uk

Nadia Kourra; WMG, University of Warwick, Coventry, CV4 7AL, UK. N.Kourra@warwick.ac.uk

Mark William; WMG, University of Warwick, Coventry, CV4 7AL, UK. M.A.Williams.1@warwick.ac.uk

Corresponding Author:

Gregory J Gibbons: WMG, University of Warwick, Coventry, CV4 7AL, UK. G.J.Gibbons@warwick.ac.uk

Abstract:

Additive Manufacturing (AM) provides an opportunity to fundamentally redesign components previously limited by conventional manufacturing techniques. A new process for this workflow of design, manufacture by Powder Bed Fusion (PBF) and validation is presented, to which a case study of a crank for a high performance racing bicycle is applied. Topology optimisation generated conceptually ideal geometry from which a functional design was interpreted. Design for AM considerations were employed to reduce build time, material usage and post-processing labour. PBF was employed to manufacture the parts, and the build quality assessed using Computed Tomography (CT). Static and dynamic functional testing was performed and compared to a Finite Element Analysis (FEA). CT confirmed good build quality of tall, complex geometry with no significant geometrical deviation from CAD over 0.5mm. Static testing proved performance close to current market leaders, although failure under fatigue occurred after just 2,495±125 cycles, the failure mechanism was consistent in both its form and location. These physical results were representative of those simulated, thus validating the FEA. This research demonstrates a complete workflow

Peer-reviewed version available at Appl. Sci. 2018, 8, 1360; doi:10.3390/app8081360

from design, manufacture, post-treatment and validation of a highly loaded PBF manufactured component, offering practitioners with a validated approach to the application of PBF.

Key Words:
Additive Manufacture; Topology Optimisation; Computed Tomography.

1: Introduction

A bicycle crankset consists of 2 cranks joined by a bottom bracket (BB), converting pedal force into rotational motion, powering the rear wheel. A typical high performance crank is box-section in form and is machined from aluminium or moulded from Carbon Fibre Reinforced Polymer. As well as low mass, high crank stiffness is also a major consideration in order to cycle more efficiently and effectively.

Solutions to achieve maximum stiffness at minimum mass are suited to topology optimisation. In addition, Additive Manufacturing (AM) offers the capability to manufacture such idealised geometry. The build quality of the complex geometry produced by AM, and the results of functional testing can both be verified by using Computed Tomography (CT), comparing a CT generated model with the CAD data e.g [1].

2: Methodology

The method developed and followed for the design, manufacture and testing of a high performance crank is given in Figure 1.

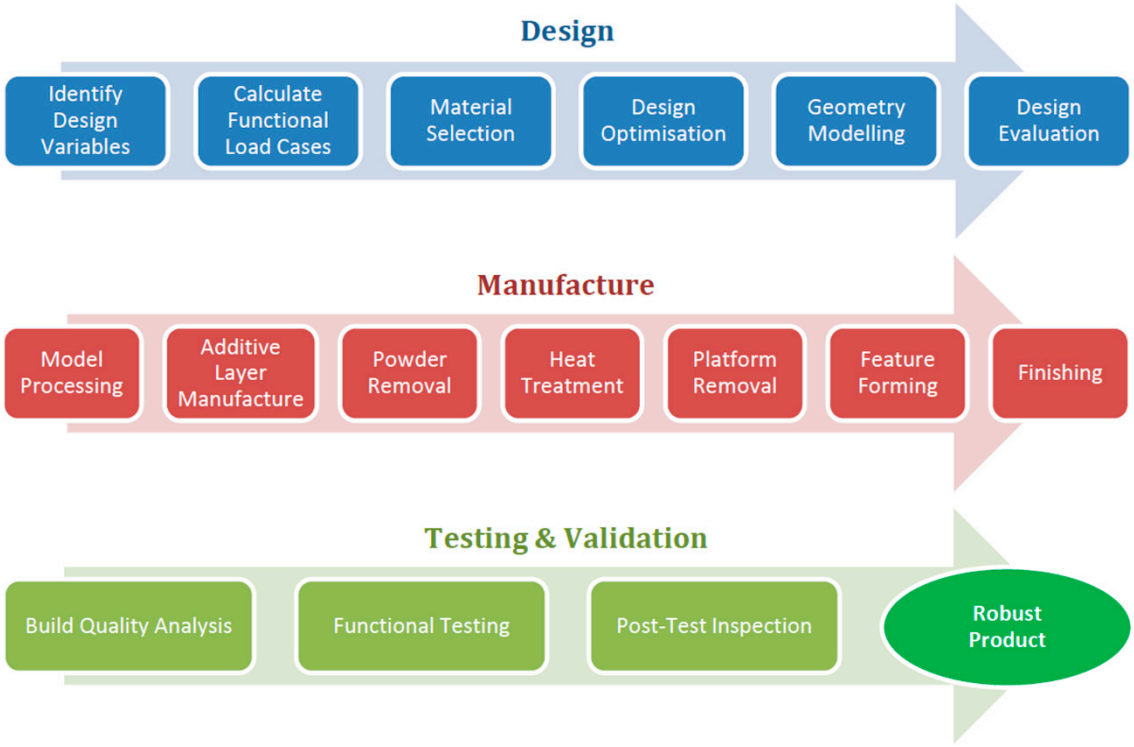

Figure 1. Crank Development Methodology.

The optimised design was benchmarked against leading metallic cranks: Hollowtech II [2] and Hollowgram SiSL2 [3] as they offer a similar cost-performance balance.

2.1: Design

Crank design began from first principles, optimising for AM whilst maximising stiffness and minimising mass. Ergonomics was considered throughout, with regards to both performance efficiency and comfort.

2.1.1: Design variables

Design variable selection was made based on a common usage and a worst-case scenario. The lower end crank boss was designed to fit a 113mm square taper cartridge Bottom Bracket (BB), BS 6102-14 (ISO 6696), with 68mm frame shell width, BS 6102-9 (ISO 6696). A top boss was designed for attachment of the pedal spindle (a 9/16" X 20 TPI British Standard Cycling Thread). The 'crank length', distance between the pedal centre spindle hole and BB taper, was set as 175mm. The distance between the outboard face of each crank was set to 147mm (standard for road products).

Preprints (www.preprints.org) | NOT PEER-REVIEWED | Posted: 17 July 2018 doi:10.20944/preprints201807.0306.v1

Peer-reviewed version available at Appl. Sci. 2018, 8, 1360; doi:10.3390/app8081360

2.1.2: Boundary conditions

Both optimisation and Finite Element Analysis (FEA) require accurate input boundary conditions. Crank assemblies must pass a 100,000 cycle fatigue test, alternating loading of each crank (set at 45°) with 1,800N 65mm from its pedal-side face (BS EN ISO 4210-8). Many studies investigate methods to model crank power. Kautz & Hull [4] defined crank force to be muscular and non-muscular (gravitational or inertial). Horizontal and vertical components of these forces at 70 rpm were used to produce a force vector profile for realistic loading [5]. This was interpolated to provide 1800N at 45° (complying with BS EN ISO 4210), with loads corresponding with numerous studies: maximum load crank angle [6] and the force vector profile (Figure 2) (hip and knee angles of 38°-50° and 73°-145°) [7] (Nasa. 2008).

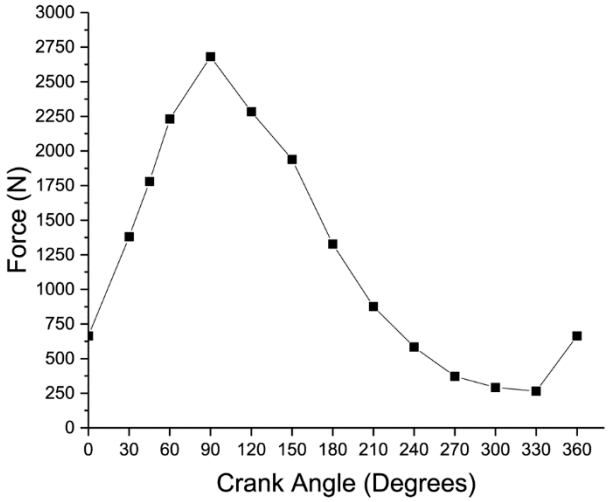

Figure 2. Force Applied to Crank at Angle.

The calculated loads were applied 65mm from the outboard crank face. A RBE3 (Rigid Body Element) connected this point to the inside face of the pedal spindle hole. This RBE represents the pedal spindle, transferring applied load to a singular external grid to the hole's face. Loads at 30° intervals were applied to ensure realistic loading and acceptable processing time. Lateral loads were not considered as with a correctly adjusted Q-Factor these would be zero.

All degrees of freedom were constrained by a Single-Point Constraint (SPC) at the centre of the square taper void. Each tapered face was connected to this with an infinitely stiff RBE2 element. This infinitely stiff RBE simulates the connection to a BB axle which cannot

undergo translational or rotational displacement. While in reality, rotation is allowed about one axis, this produces an unsolvable model for optimisation and this configuration may thus produce an overly-stiff result.

2.1.3: Material selection

A high specific stiffness and specific strength is required for high performance at low mass. Therefore density, Young's Modulus and Yield Strength were identified as key factors. Based on these requirements, Titanium Ti64 and Maraging Steel MS1 are the most favourable options [8] (Table 1).

Parameter	EOS Ti64	EOS MS1
Density (g/cm^3)	4.41	8.05
Young's Mod. (GPa)	115 ± 10	180 ± 20
Yield Strength (MPa)	860 ± 20	1990 ± 100

Table 1. EOS Material Properties [9, 10]

2.1.4: Optimisation

Topology optimisation was selected as it provides a conceptual geometry for design development. In this case, the design objective was to produce maximum stiffness at minimum mass.

The size of the design space (Figure 3) was limited by physical realities during cycling. Firstly, the limb of the cyclist prevents any protrusions on the pedal-side of the crank so the design space was trimmed in accordance with the Q-Factor and an approximate foot width. The opposite side was made parallel to a hypothetical chain stay to prevent contact with the frame.

Peer-reviewed version available at Appl. Sci. 2018, 8, 1360; doi:10.3390/app8081360

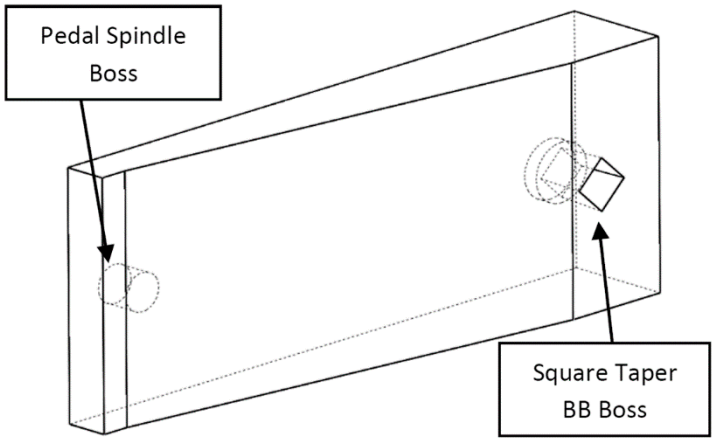

Figure 3. Design Space (view from inboard side).

HyperMesh 13.0 (Altair Engineering, UK) was used to pre-process and mesh the geometry created in CAD. Genesis Design Studio 14.0 (GRM Consulting, UK) was used to perform the optimisation. The Boundary Conditions (2.1.2) were inputs into the model. The mechanical properties of Ti64 were used as the material of choice. Elements of the model were separated into Design Space (DES) (optimised) and Fixed Geometry (FIX) (non-optimised), given as red and blue respectively. The model configuration can be seen Figure 4.

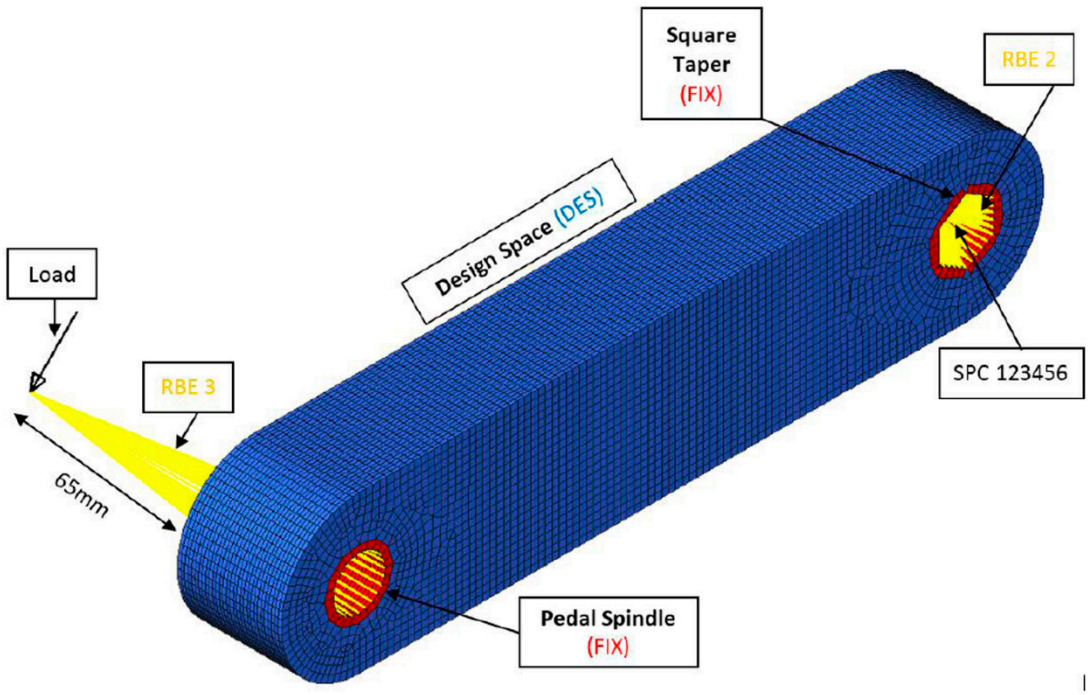

Figure 4. Topology Optimisation Model Configuration.

Peer-reviewed version available at Appl. Sci. 2018, 8, 1360; doi:10.3390/app8081360

Since AM enables freeform manufacture, no manufacturing constraints were imposed. The design objective was set to minimise strain energy (maximising stiffness). Mass was also defined as a design objective, the 'weighting' of which was increased with progressive iterations.

A relatively coarse initial mesh was used to increase optimisation efficiency. Once reasonable results were obtained, the mesh was refined, increasing the number of tetrahedral elements 10-fold to 504,495 (average element size of 1.09mm^2), increasing the accuracy of the resulting isosurfaces (the surface form of the topology optimisation).

2.1.5: Geometry creation and computer aided design

The isosurfaces were exported from Design Studio as an STL file and imported into SolidWorks 2015 (Dassault Systèmes, France) and directly traced over to produce a practical crank model.

Consideration of AM build direction influenced the development of the design. A vertical build direction starting from the BB boss was selected based on the geometry to reduce the likelihood of manufacturing defects as well as maximising yield.

2.1.6: Design evaluation

FEA was performed in SolidWorks Simulation 2015 (Dassault Systèmes, France) for each load case; two methods were predominantly used as they would be ultimately replicated by physical testing.

The first test was conducted to provide benchmarking information. Benchmark data for the Hollowtech II and Hollowgram SiSL2 [11] was used, collected by setting the crank at 90°, applying 890N (225N preload and 667.5N main load) 60mm from the outboard face. This method was repeated 3 times per crank and the average deflection (due to main load) published.

Secondly, the BS EN ISO 4210-8 fatigue test parameters described in 2.1.2 were replicated in a static scenario in order to analyse the response of the part under loading.

2.2: Manufacture

2.2.1: Model pre-processing

To improve the stability of the build, a solid block base was added to the bottom of the part. The CAD model was exported as an STL file and imported into Magics v19.0 (Materialise Ltd, UK) and support material was generated for the pedal spindle hole as well as the square taper (Figure 5 - support material in red). The solid bar was included for calibration of the wire EDM machine for accurate part removal from the build plate.

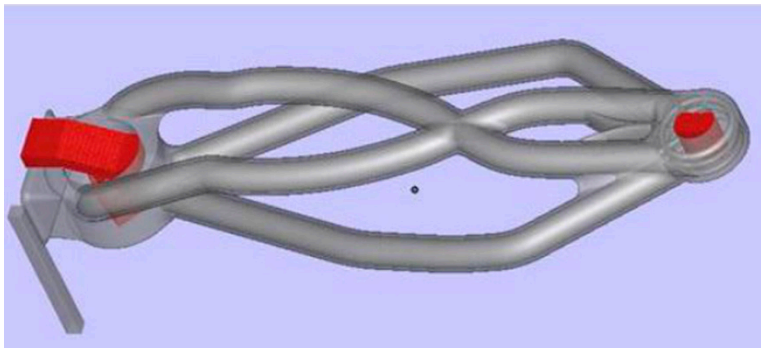

Figure 5. Build Model.

2.2.2: Additive manufacturing

Parts were manufactured on an EOS M280 (EOS GmbH, Germany) in 60µm layers using standard parameters “Ti64_060_110 Speed” and HSS steel re-coater blade. Powder was sieved using the EOS IPCM-M equipment to <63µm from a single batch of Ti64 (EOS GmbH, Germany). The finished build prior to its removal from the machine can be seen in Figure 6.

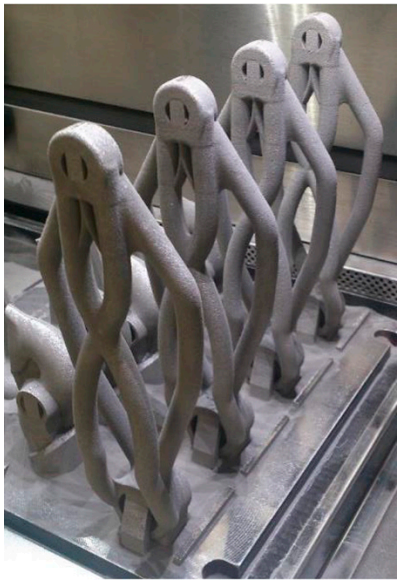

Figure 6. Built Parts in Machine.

Peer-reviewed version available at Appl. Sci. 2018, 8, 1360; doi:10.3390/app8081360

2.2.3: Powder removal

Once out of the machine, a hydraulic line was attached securely to the build platform to deliver short pulses which produced a vibration in the plate and thus the parts, improving the effectiveness of material removal. The plate was manipulated by hand to ensure that all loose powder had been evacuated.

2.2.4: Post-treatment

The parts were heat treated (Tamworth Heat Treatment Ltd, UK) at 800°C for 4 hours in a vacuum [9] to reduce anisotropy [12]. Heat treatment also reduces yield strength, increases elastic modulus, and most importantly, improves fatigue properties.

The components wire EDM were removed from the build platform and the square taper cut into the BB boss (Exetek V500G) (Exeteck Technologies Ltd., Taiwan). The pedal spindle boss was tapped using an ISO M12 tap. As this was a worst-case scenario design, no surface finishing processes were carried out as this would improve the fatigue characteristics of the components [13].

2.3: Validation

2.3.1: Post-manufacture inspection

CT Scanning of the part removed from the build plate was completed using an X- Metris TEK XTH 320 LC (Nikon Metrology, UK). The exposure was set to 300kV or 40W for a time of 4s, a magnification of x1.8 and a gain of 24dB and a 2mm Sn filter. The CT scan (3145 projections over 20 hours) used a voxel size of 111.11µm and unsharpness size of 114.05µm.

The digital 3D model ‘actual model’ from the scan was compared to the CAD ‘nominal model’. The actual and nominal models were aligned using the datum method. The flat faces of the BB boss were used as a datum as they were the most stable during the build and having best flatness, parallelism and dimensional accuracy. A secondary “best fit” method was also used, where an algorithm fitted the models together by identifying the greatest number of common surface points.

2.3.2: Functional validation

Physical testing was conducted to BS EN ISO 4210 by Bureau Veritas UK Ltd, using a hydraulic rig to test.

2.3.2.1: Static loading. This test was conducted to benchmark against the Fairwheel Bikes data [11] with the crank set at 90°, 890N was applied at 65mm (5mm further out than the simulation) from the outboard face (Figure 7). A fixed identical Crank was placed on the opposite end of the axle to prevent rotation. The magnitude of deflection was manually measured with a steel rule on the crank itself at the pedal spindle boss.

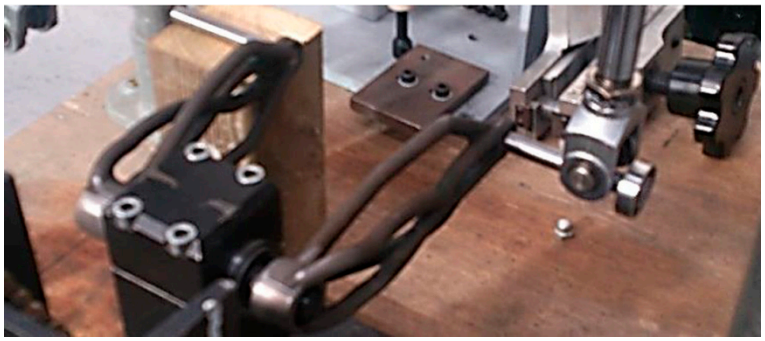

Figure 7. Static Test Configuration.

2.3.2.2: fatigue. The crank (set at 45°) was loaded with 1,800N 65mm from its outboard face (Figure 8) at 0.5Hz (1s force on; 1s force off). A solid commercial crank was used to prevent rotation. Two samples from the same PBF build were tested.

Figure 8. Fatigue Test Configuration.

3: Results and discussion

3.1: Material selection

Both Ti64 and MS1 exhibit excellent specific properties, however, while the exceedingly high strength of Maraging Steel MS1 may enable a lower mass to be used for a similar performance, its reduced ductility may degrade the fatigue capability of the component. Therefore, Ti64 was selected as the material of choice.

3.2: Optimisation

The topology optimisation isosurface results produced are given in Figure 9. Theoretically, this is the ideal design of a solid crank with increasing levels of weight reduction. The complex geometry shown suggests that ALM would be the favoured, if not the only possible method of manufacture for producing this design.

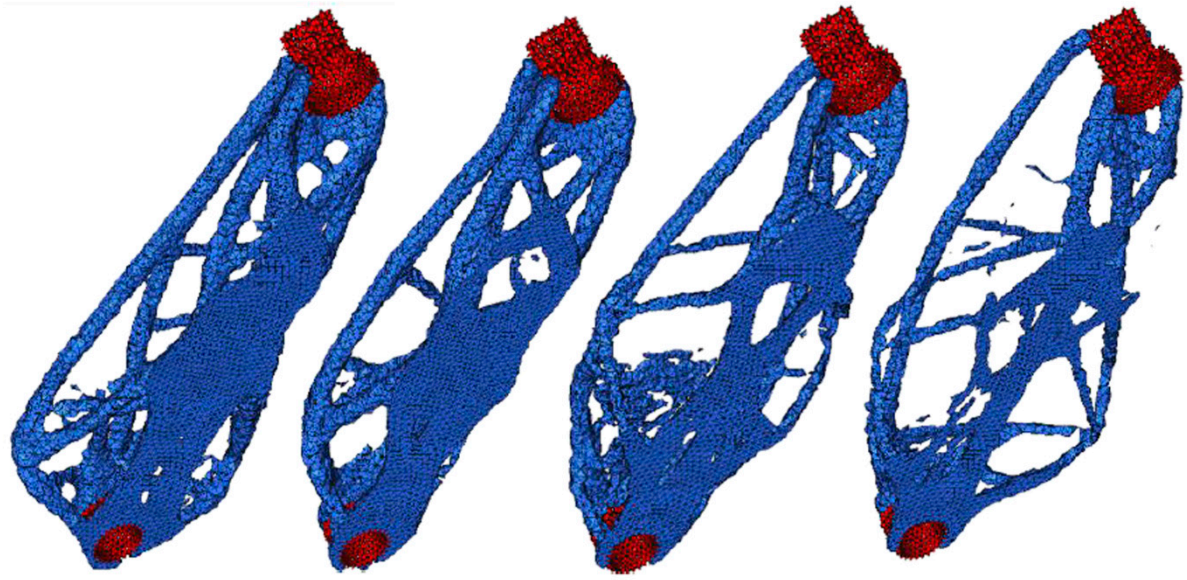

Figure 9. Topology Optimisation Isosurface Results (Increasing Mass Reduction Top to Bottom).

3.3: Geometry creation & computer aided design

It is clear from Figure 9 that the results from the optimisation could not simply be printed. "Design interpretation" is a key stage of this process; using some of the optimisation results directly may implement too high a level of mass reduction which may not perform functionally. In order to account for this, common features present in all results were identified. These could then be traced in CAD, at which stage each feature could be easily modified using FEA guidance to reach the optimal level of mass reduction. These common

Peer-reviewed version available at Appl. Sci. 2018, 8, 1360; doi:10.3390/app8081360

features included the 4 primary "limbs" as well as the "auxiliary spars" stemming from these (highlighted yellow and pink respectively in Figure 10).

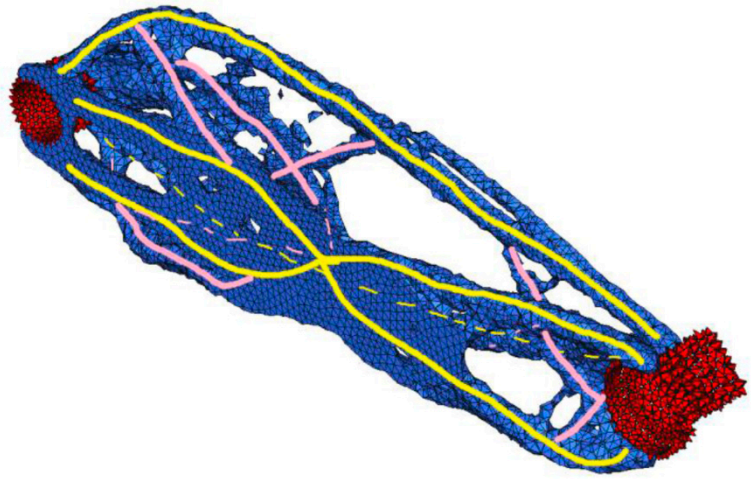

Figure 10. Design Interpretation.

The design interpretation produces beam-like structures which can fail through fracture or deflection; determined by their strength and stiffness respectively. In pure bending, the value for second moment of area (I) is key, where a greater I decreases stress and deflection. Torsion however is dependent upon the polar second moment of area (J), where a greater J reduces shear stress and twist. J should be maximised for strength and stiffness [14]. Application of this theory identified three design variables:

(1) Tube Diameter 'D' :- ↑D=↑J; ↑Mass
(2) Wall Thickness 'WT':- ↑WT=↓J; ↑Mass
(3) Auxiliary Tubing :- Addition as per topology results.

As this was a feasibility assessment with regards to building the component, a "worst-case" of these variables was used.

3.3.1: Design for Additive Manufacturing

The current design is produced entirely through focusing on performance; modifications have to be made with regards to Design for Additive Manufacture (D4AM) (Figure 11). Due to its complex geometry, support material would likely be removed by hand and thus be time consuming and uneconomical. Therefore all proceeding design work aimed to require no further support material for manufacture (now only required at the pedal spindle, BB taper and base), reducing waste material, cost and build time.

Peer-reviewed version available at Appl. Sci. 2018, 8, 1360; doi:10.3390/app8081360

A feature was added to support the bottom of the pedal spindle boss (Figure 11). To enable powder removal from inside the part, holes were routed through the component.

The model was heavily filleted both internally and externally to ease stress concentrations and reduce the risk of manufacturing defects. The fillet radius was dependent upon the geometry of the feature, external radii were matched by corresponding internal fillets to achieve uniform wall thickness throughout.

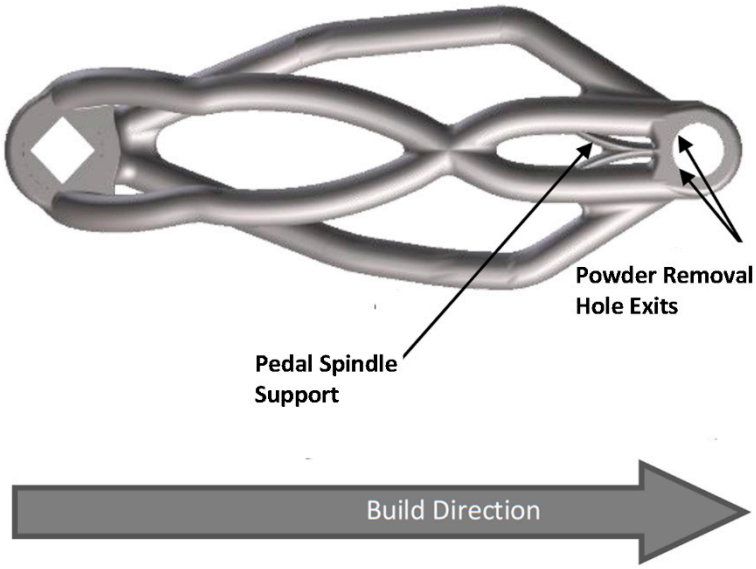

Figure 11. D4AM Diagram.

3.4: Design evaluation

Inconsistencies between the Fairwheel test method [11] and the simulation exist. Fairwheel used a 222.5N preload before increasing to 890N, reporting deflection between these two values. The simulated deflection however will include preload deflection. The simulation used fixed constraints on the square taper faces, whereas in the actual test this is connected to a BB and therefore torsion and bending of this component is not accounted for in the simulated results, whilst approximately 70% of total deflection measured at the pedal comes from axle twist [15] (Huang. 2017). Finally, the Fairwheel test deflection was measured with force applied to the pedal spindle, thus including deformation of the pedal spindle in its measurement. The results are shown in Figure 12-a, with a resultant displacement of 2.258mm.

The fatigue test was replicated identically in SolidWorks as per BS EN ISO 4210. While this also used fixed constraints on the square taper faces, this would only increase the stress levels

Preprints (www.preprints.org) | NOT PEER-REVIEWED | Posted: 17 July 2018 doi:10.20944/preprints201807.0306.v1

Peer-reviewed version available at Appl. Sci. 2018, 8, 1360; doi:10.3390/app8081360

and therefore produce a worst-case. Accounting for this, no regions of the results (see Figure 12-b) were significantly beyond the yield stress value.

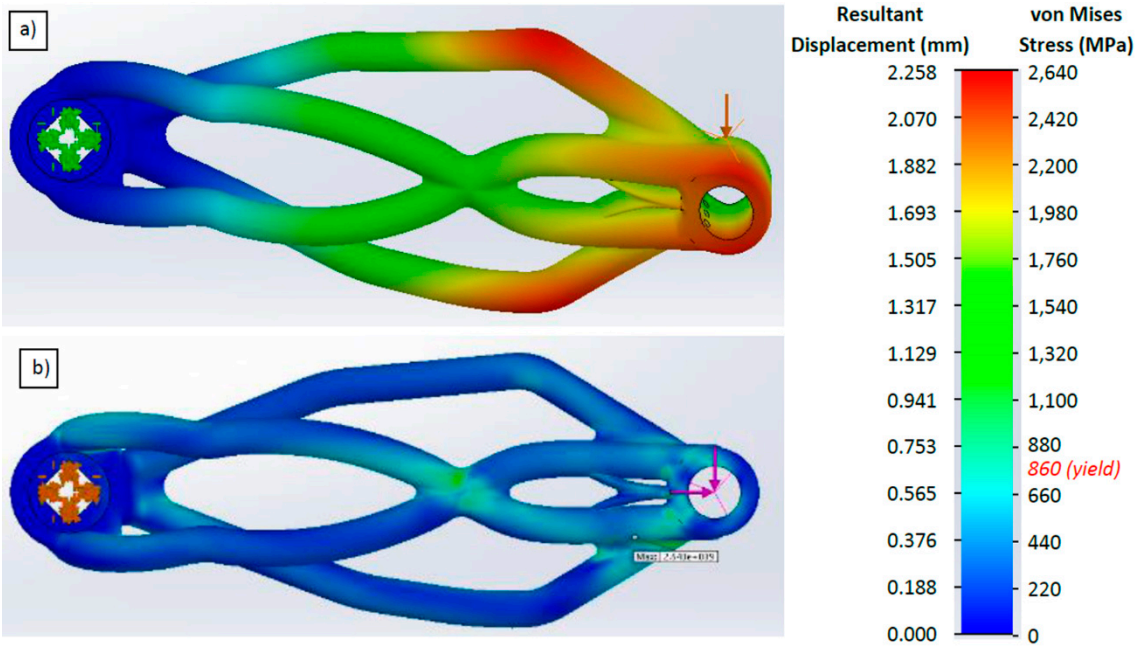

Figure 12. a) Static Test Using Fairwheel Bikes Method (Resultant Displacement); b) Static Test Using Fatigue Parameters (von Mises Stress).

3.5: Powder removal

As this process was performed manually, it was difficult to ensure that all powder was completely removed from the internals of the component. Examination of the CT scanned layers showed no signs of powder remaining within the structure, confirming that powder removal routes were satisfactory.

3.6: Post-manufacture inspection

The datum method showed significant differences at the top of the part. The best fit method however produced lower levels of variation (Figure 13). The variance distribution % for both methods is given in Figure 14, where the datum method results in a significant % exceeding 0.5mm deviation, whereas the best fit does not significantly exceed 0.3mm.

Preprints (www.preprints.org) | NOT PEER-REVIEWED | Posted: 17 July 2018 doi:10.20944/preprints201807.0306.v1

Peer-reviewed version available at Appl. Sci. 2018, 8, 1360; doi:10.3390/app8081360

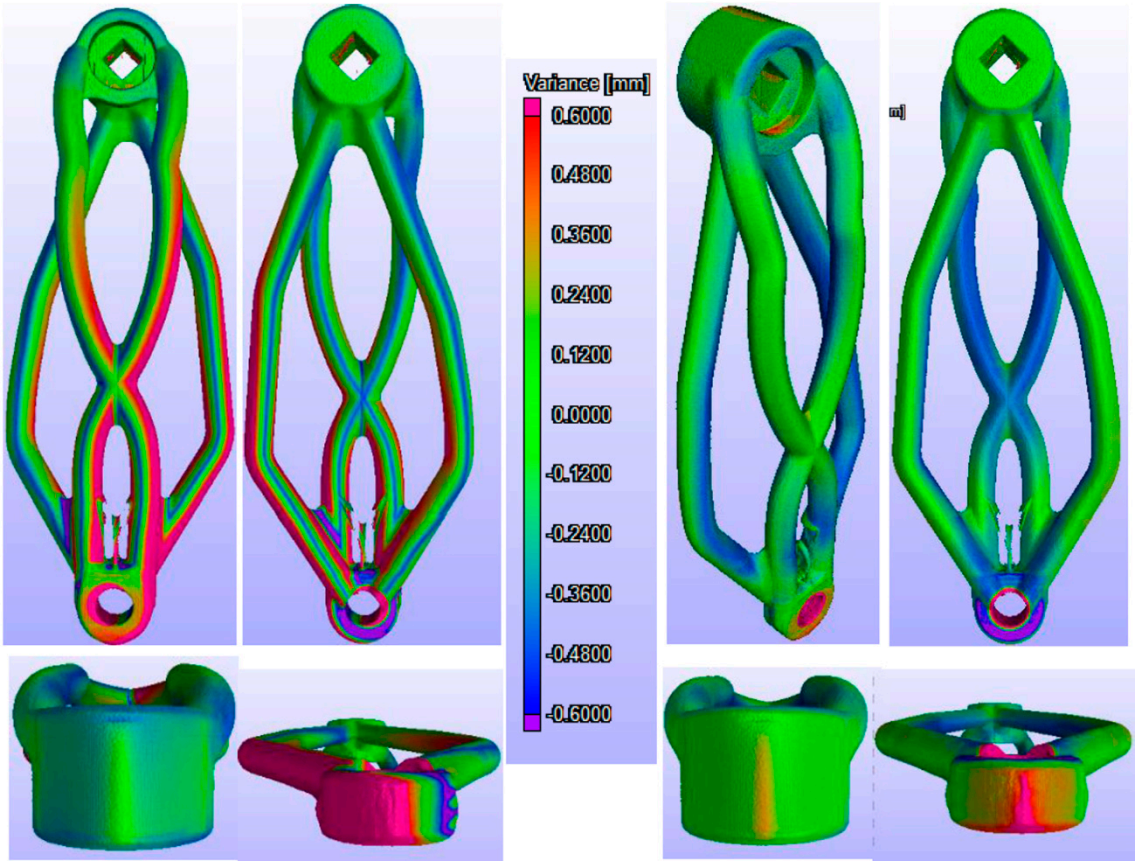

Figure 13. Comparison of Actual and Nominal Models; Left: Datum-Reference Method; Right: Best Fit Alignment Method.

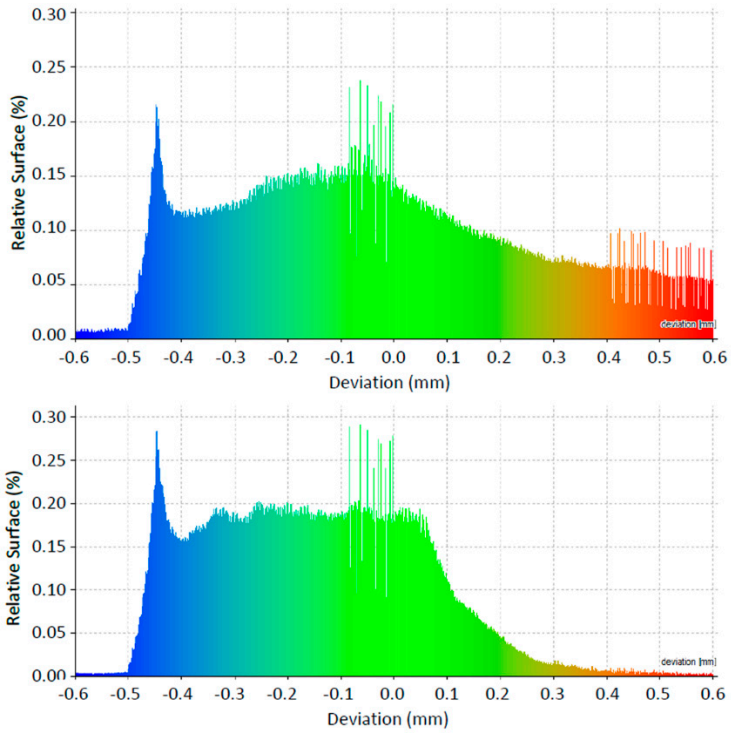

Figure 14. Percentage Variation Distribution for Top: Datum Method; Bottom: Best Fit Method.

Peer-reviewed version available at Appl. Sci. 2018, 8, 1360; doi:10.3390/app8081360

The maximum geometry variance of under 1mm is deemed insignificant with regards to its application, and therefore build quality is acceptable. The majority of the deviation is most likely caused by re-coater blade contact during the PBF powder layering process as opposed to the effect of residual stresses.

Scans of the internal geometry confirmed that the wall thickness produced is identical to the desired value (Figure 15). Modelling of the pedal spindle support was affected by CT noise reduction algorithms and threshold selection and, due to its smaller wall thickness, geometry comparison of this feature was limited.

Figure 15. CT Scan of Primary Limb Confirming Wall Thickness.

3.7: Functional validation

3.7.1: static loading

Under the Fairwheel Bikes method, the crank deflection was 14.0±0.5mm. As an identical crank was used to prevent rotation on the opposite side it can be assumed that this deformed equally, therefore producing a deflection of 7.0±0.5mm per crank. Twisting of the part could not be accounted for. Lateral displacement occurs at the red patches during simulation seen on the rear main tubes in Figure 5, suggesting twisting of the crank under load, and therefore this effect is not insignificant but is not being recorded in its own right.

The simulation of this method produced a deflection of just 2.258mm (c.f 7.0±0.5mm). It is likely that much of this deviation is due to the simulation not measuring torsion of the BB.

This is reinforced by claims that roughly 70% of deflection is due to BB torsion (Huang. 2017), with the simulated value of 2.258mm being 32% of the measured value.

A comparison of this design with the benchmark cranks is given in Table 2 and indicates that this worst-case design for the AM crank is stiffer than current market leading designs, and at a competitive weight.

Parameter	Shimano	Cannondale	AM
Mass (g)	175	125	155
Deflection (mm)	7.67*	6.91*	7.0±0.5

* 50ib-200lb distance only [11]

Table 2. Benchmarked Results.

3.7.2: Fatigue

Both of the tests completed each failed catastrophically, through identical mechanisms, after similar durations (2,370 and 2,620 cycles) (Figure 16). During the design phase yield stress (860MPa) had been used as the mechanical limit, whereas the actual capability of a part under fatigue is lower than this. Rekedal [16] investigated high cycle fatigue life of Ti64 using identical build and heat treatment parameters to those here. The Rekedal study shows that suggests that peak stress below 250MPa would be required to achieve 100,000 cycles. Edwards and Ramulu [12] found that we would expect failure earlier than physically occurred.

The fatigue configuration was simulated in a static test (Figure 12-b). At the centre section where critical failure occurred, a higher stress can be seen (green). Combining this with the components post-fatigue (Figure 16), it is likely that the fracture initiated at this location and propagated across the part under cyclic loading. The other non-critical area of damage (Figure 16), is also a region of higher stress. The area located near the pedal spindle however, where the maximum stress is identified, showed no signs of external damage, although this is an area of high material concentration and therefore had better stress-relieving characteristics.

Peer-reviewed version available at Appl. Sci. 2018, 8, 1360; doi:10.3390/app8081360

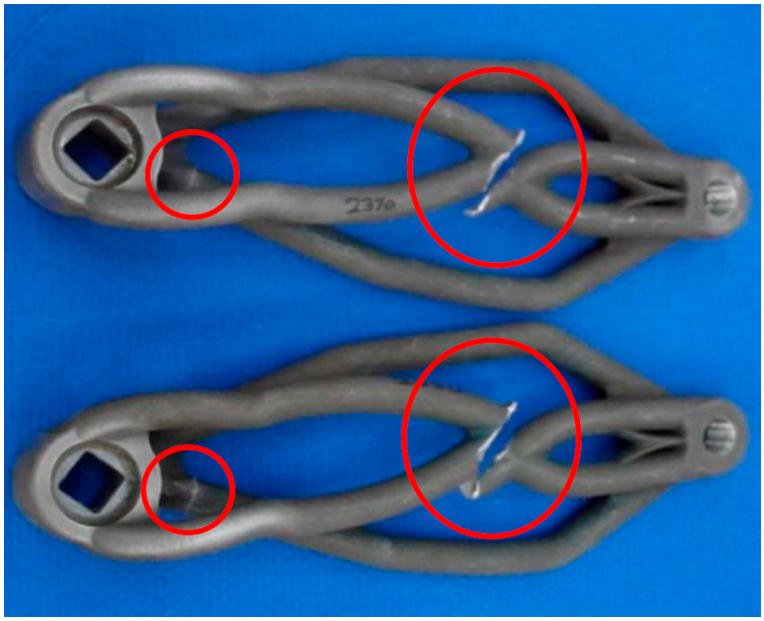

Figure 16. Damage Identification from Fatigue; Left: N=2,370, Right: N=2,620.

4: Conclusions

Topology optimisation produced a design which would unlikely to have been produced by human design, increasing the efficiency and effectiveness of the design phase significantly, whilst increasing functional performance.

PBF was used to successfully build the topology optimised design, impossible using conventional manufacturing techniques.

CT Scanning was used to successfully validate acceptable build quality of a tall complex design achieved using minimal supports.

This worst-scenario design performed within the region of market leader products, design development of which will likely see their performance exceeded.

Incorporation of biomechanics specific to the realistic loading conditions enabled the production of a product which has the potential to outperform more conventional designs.

FEA simulation was used to diagnose catastrophic failure of the part under fatigue, giving confidence that it provides an accurate representation of a component produced by ALM.

5: Acknowledgements

The authors wish to thank the High Value Manufacturing Catapult for supporting this research.

6: References

1. Cooper, D., Thornby, J., Blundell, N., Henrys, R., Williams, M.A., Gibbons, G. Design and Manufacture of High Performance Hollow Engine Valves by Additive Layer Manufacturing. *JMAD,* **2015**, *69*, 44-55, doi.org/10.1016/j.matdes.2014.11.017.

2. Hollowtech II Crankset. Available online: bike.shimano.com/en-EU/technologies/component/details/hollowtech-2.html (accessed 16/07/2018).

3. Hollowgram SiSL2 Road. Available online: www.cannondale.com/en/USA/Gear/GearDetail?Id=cbde5cb1-afbe-4b34-b6ff-3c11b51c8870 (accessed 16/07/2018).

4. Kautz, S.A., Hull. M.L. A Theoretical Basis for Interpreting the Force Applied to Pedal in Cycling. *J BIOMECH,* **1993**, *26,* 2, 55-165, doi.org/10.1016/0021-9290(93)90046-H.

5. Bertuccia, W., Grappea, F., Girarda, A., Betikab, A., Rouillonc, J.D. Effects on the Crank Torque Profile when Changing Pedalling Cadence in Level Ground and Uphill Road Cycling. *J BIOMECH,* **2005**, *38*, 2, 1003-1010, doi.org/10.1016/j.jbiomech.2004.05.037.

6. Bini, R.R., Humea, P.A., Cerviric. A. A Comparison of Cycling SRM Crank and Strain Gauge Instrumented Pedal Measures of Peak Torque, Crank Angle at Peak Torque and Power Output. *PROCEDIA ENGINEERING,* **2011**, *13*, 56-61, doi.org/10.1016/j.proeng.2011.05.051.

7. Human Performance Capabilities. Available online: msis.jsc.nasa.gov/sections/section04.htm#_4.9_STREN GTH. (accessed 16/7/2018).

8. Materials for Metal Manufacturing. Available online: www.eos.info/material-m. (accessed 16/07/2018).

9. Ti64 Material Data Sheet. Available online: cdn.eos.info/a4eeb73865d54434/5926811b3739/Ti-Ti64_9011-0014_9011-0039_M290_Material_data_sheet_11-17_en.pdf (accessed 26/07/2018).

10. MS1 Material Data Sheet. Available online: www.eos.info/material-m/download/material-datasheet-eos-maragingsteel-ms1.pdf (accessed 26/07/2018)

11. Road Bike Crank Test. Available online: blog.fairwheelbikes.com/reviews-and-testing/road-bike-crank-testing. (accessed 16/07/2018).

12. Edwards, P. and Ramulu. M. Fatigue Performance Evaluation of Selective Laser Melted Ti-6Al-4V. **2014**. *MAT SCI ENG A-STRUCT, 598*, 327-337, doi.org/10.1016/j.msea.2014.01.041.

13. Greitemeier, D., Dalle Donne, C., Syassen, F., Eufinger, J., Melz, T. Effect of Surface Roughness on Fatigue Performance of Additive Manufactured Ti–6Al–4V. *MATER SCI TECH SER*, **2013**, *53*, 629-634, doi.org/10.1179/1743284715Y.0000000053.

14. Budynas R.G., Nisbett, K.J. *Shigley's Mechanical Engineering Design*. McGraw-Hill, London, UK, 2011.

15. BikeRadar: Complete Guide to Bottom Brackets. Available online: www.bikeradar.com/gear/article/complete-guide-tobottom-brackets-36660. (accessed 13/08/2017).

16. Rekedal, K. D. Investigation of the High-Cycle Fatigue Life of SLM and HIP Ti-6Al-4V. MSc, Ohio Air Force Institute of Technology, USA, 2015.